coatings

MDPI

Article

Preparation of Hydroxyapatite/Tannic Acid Coating to Enhance the Corrosion Resistance and Cytocompatibility of AZ31 Magnesium Alloys

Bowu Zhu [1], Shimeng Wang [1], Lei Wang [1], Yang Yang [1], Jun Liang [2,*] and Baocheng Cao [1,*]

[1] School of Stomatology, Lanzhou University, Lanzhou 730000, China; zhoubw10@lzu.edu.cn (B.Z.); wangshm16@lzu.edu.cn (S.W.); wanglei2016@lzu.edu.cn (L.W.); yangyang16@lzu.edu.cn (Y.Y.)

[2] State Key Laboratory of Solid Lubrication, Lanzhou Institute of Chemical Physics, Chinese Academy of Sciences, Lanzhou 730000, China

* Correspondence: jliang@licp.cas.cn (J.L.); caobch@lzu.edu.cn (B.C.); Tel.: +86-931-496-8851 (J.L.); +86-931-891-5051 (B.C.)

Received: 13 June 2017; Accepted: 18 July 2017; Published: 20 July 2017

Abstract: Hydroxyapatite/tannic acid coating (HA/TA) were prepared on AZ31 magnesium alloys (AZ31) via chemical conversion and biomimetic methods. The characterization and properties of the coating were studied by scanning electron microscopy (SEM), X-ray diffraction (XRD), Fourier transform infrared spectroscopy (FTIR), corrosion testing, MC3T3-E1 cell proliferation assay, and MC3T3-E1 cell morphology observation. The results showed that tannic acid as an inducer increased the number of nucleation centers of hydroxyapatite and rendered the morphology more uniform. Compared to bare AZ31 magnesium (Mg) alloys ($E_{corr} = -1.462 \pm 0.006$ V, $I_{corr} = (4.8978 \pm 0.2455) \times 10^{-6}$ A/cm^2), the corrosion current density of the HA/TA-coated magnesium alloys ($(5.6494 \pm 0.3187) \times 10^{-8}$ A/cm^2) decreased two orders of magnitude, and the corrosion potential of the HA/TA-coated Mg alloys ($E_{corr} = -1.304 \pm 0.006$ V) increased by about 158 mV. This indicated that the HA/TA coating was effectively protecting the AZ31 against corrosion in simulated body fluid (SBF). Cell proliferation assays and cell morphology observations results showed that the HA/TA coating was not toxic to the MC3T3-E1 cells.

Keywords: biomimetic; hydroxyapatite; tannic acid; magnesium alloy; corrosion; cytocompatibility

1. Introduction

Compared with other metal materials for the current clinical application, magnesium alloys have some good advantages, such as their recoverability, lightweight nature, good mechanical strength, and good resistance against electromagnetic waves [1–4]. In particular, their elastic modulus is similar to natural bone tissue and can prevent the occurrence of stress shielding effects to facilitate the healing of bone tissue [2]. In addition, magnesium alloys have good biodegradable properties, which can avoid surgical removal of implants at the end of the treatment. This reduces the economic burden and health risks of patients [2]. Therefore, magnesium alloys have recently attracted attention as an implant material for orthopedic surgery and cardiovascular medicine [4–6]. However, magnesium alloys also have a very negative potential and poor corrosion resistance, which influences bone bonding and suppresses their development for biomedical applications [7].

To overcome these shortcomings and increase cytocompatibility, magnesium alloys are usually coated with bone-integrating or bone-inducing biological materials, such as hydroxyapatite (HA) [8–10]. HA coating on Mg alloys is prepared through many methods, such as sputter coating, pulsed laser deposition, sol-gel techniques, biomimetic coatings, and electrophoretic deposition [11–15]. Of these methods, the method of biomimetic mineralization is simple, easy to operate, and inexpensive.

In addition, the method of biomimetic mineralization can not only prepare a bone-like apatite coating on the surface of materials which have a complicated shape, but can also add bone growth-stimulating factors to the coating [16]. However, due to a lack of nucleation centers for hydroxyapatite growth, direct biomimetic deposition of hydroxyapatite on untreated AZ31 magnesium alloy is very difficult [17]. Furthermore, the mechanical properties and chemical stability of the directly-prepared coating are deficient [18]. To solve these problems, organic additives can be applied to induce and accelerate the growth of HA [19,20].

Tannic acid ($C_{76}H_{52}O_{46}$) as an organic compound can react with metal ions to form tannic acid-metal complexes. Therefore, tannic acid is used to prepare coatings to enhance the corrosion resistance of stainless steel in the 19th century and early 20th century [21]. Recently, tannic acid has again attracted attention as a coating for aluminum, aluminum alloys, stainless steel, and magnesium alloys via chemical conversion methods to increase their corrosion resistance [22–24].

However, the use of tannic acid as an inducer to prepare a hydroxyapatite coating on the surface of AZ31 magnesium alloys has not yet been reported. Our work explores the possibility of preparing hydroxyapatite coatings on the surface of AZ31 magnesium alloys with the assistance of tannic acid via biomimetic mineralization, and further improves the corrosion resistance and cytocompatibility of magnesium alloys.

2. Materials and Methods

2.1. Sample Preparation

The AZ31 magnesium alloys specimens were cut into 10 mm × 10 mm × 1 mm plates. The samples were mechanically polished using 600–1200 grit SiC abrasive papers. The samples were cleaned in acetone and anhydrous ethanol for 5 min each in an ultrasonic bath. All specimens were rinsed by using deionized water and dried in air. All samples were soaked in 1 mol/L NaOH solution for 24 h and then were heated at 150 °C in air for 1 h in a muffle furnace before the preparation of the tannic acid coating. This stabilized the surface of the AZ31 magnesium alloy [4,25].

2.2. Preparation of Tannic Acid Coating (TA) on AZ31 Mg Alloys

According to Chen et al. [26], a tannic acid coating was formed on the surface of pretreated AZ31 magnesium alloy via chemical conversion. Tannic acid conversion solution was configured by 0.05 g Na_3PO_4, 0.25 g $Na_2B_7O_4$, 0.04 g $C_{76}H_{52}O_{46}$, 0.05 g NH_4VO_3, 0.055 g K_2ZrF_6, and 0.02 g HNO_3 added in 50 mL deionized water. The pH of the solution was adjusted to 4 with HNO_3. Subsequently, the samples were soaked in the tannic acid solution and then preserved in a constant temperature box at 37 °C for 9 h. Finally, the samples were washed twice by deionized water and then dried in air at room temperature, and then a visible and tawny coating formed on the AZ31 magnesium. The result is consistent with the result of Chen et al. [26].

2.3. Tannic Acid Coating-Assisted HA Formation

The calcium phosphate (CaP) solution was configured according to the Gui description [4]. The concentration of $Ca(NO_3)_2$, NaH_2PO_4, and $NaHCO_3$ in the CaP solution was 14 mmol/L, 8.4 mmol/L, 4 mmol/L, respectively. The tannic acid-coated substrate (TA/AZ31) was immediately soaked in the CaP solution and placed in a constant temperature box for 48 h at 37 °C to assist the growth of CaP crystals. The CaP solution was replaced every 24 h. Then, the samples (HA/TA/AZ31) were rinsed with deionized water and dried in air at room temperature. Furthermore, the bare AZ31 was directly soaked in the CaP solution with the above method to prepare the HA coating on the AZ31 (HA/AZ31).

2.4. Surface Characterization

The corresponding characterization of the sample groups including AZ31, TA/AZ31, HA/AZ31, and HA/TA/AZ31 were performed by scanning electron microscopy (SEM), X-ray diffraction (XRD),

Fourier transform infrared spectroscopy (FTIR), and energy-dispersive X-ray spectroscopy (EDS). In order to observe the cross-sectional morphology of the samples under the scanning electron microscope, the samples were embedded in resin, and were then polished using 600–7000 grit SiC abrasive papers to expose the cross-section. Scanning electron microscopy (SEM; Hitachi S-4800, Hitachi, Ltd., Tokyo, Japan) was used to observe the sample surface and cross-sectional morphology. The distance from the interface of AZ31 magnesium alloy and its coating to the interface of the coating and the resin was measured by Image-Pro Plus 6.0 (version 6.0.0.260, Media Cybernetics, Inc., Bethesda, MD, USA, 2006), that is to say, the measurement was the thickness of the coating. We selected 10 different positions in each group to complete the above measurement. The results were expressed in the form of mean value ± standard deviation. The elemental compositions of the samples also were analyzed with energy-dispersive X-ray spectroscopy (EDS; Hitachi S-4800, Hitachi, Ltd., Tokyo, Japan). To specify the phase structure of the coating, X-rays diffractometry (XRD, D/MAX-2400, Rigaku Co., Ltd., Tokyo, Japan, λ = 0.154181 nm) with Cu Kα radiation was used at room temperature. The range of test angle (2θ), voltage, current, and the step length were 20° to 80°, 40 kV, 150 mA, and 0.02°, respectively. In addition, the characteristic functional groups of all samples were detected by Fourier transform infrared spectroscopy (FTIR; Nicolet, Madison, WI, USA) with acquisition range from 4000 to 500 cm^{-1}, and a scan resolution of 4 cm^{-1}. The FTIR experiments were performed on the pellet specimens, which were obtained by mechanically scratching the film from the substrate and mixing the obtained powder with KBr.

2.5. Corrosion Evaluation

2.5.1. Electrochemical Measurements

The potentiodynamic polarization test and electrochemical impedance spectroscopy were performed in a three-electrode cell and electrochemical workstation (Autolab PGSTAT302N, Metrohm, The Netherlands) to evaluate the corrosion resistance of samples (AZ31, TA/AZ31, HA/AZ31, and HA/TA/AZ31). The corrosion solution was simulated body fluids (SBF), which was prepared according to Kokubo and Takadama [27]. Here, the SBF temperature was controlled at 37 °C. The working electrode, reference electrode, and the counter electrode were the specimen, an Ag/AgCl electrode (saturated with KCl), and a titanium plate, respectively. Before the start of the electrochemical test, the sample was soaked in SBF solution for 600 s to obtain a stable open circuit potential. The potentiodynamic polarization curve was obtained under a scanning rate of 1 mV/s. The electrochemical impedance spectrum frequency range was 0.01 Hz to 100,000 Hz, and the results were analyzed by ZView 2 (version 2.9c, Scribner Associates, Southern Pines, NC, USA, 2005) software. The exposed sample area was 0.5 cm^2 in SBF. To ensure the repeatability of experimental results, the experiment was repeated three times. The corrosion potential (E_{corr}) and corrosion current density (I_{corr}) of the AZ31, TA/AZ31, HA/AZ31, and HA/TA/AZ31 were also subjected to unpaired single tailed Student's *t*-test. A value of $p < 0.05$ was considered as significant.

2.5.2. Immersion Tests

The immersion test with hydrogen evolution was a simple and inexpensive way to measure corrosion behavior [28]. According to Bakhsheshi-Rad [28], immersion test was performed in SBF for seven days. Specimens (AZ31, TA/AZ31, HA/AZ31, and HA/TA/AZ31) were immersed in a beaker containing 800 mL of SBF, where a funnel was located over the samples to collect evolved hydrogen in a burette (50 mL) placed above the funnel. During the experiment, the hydrogen release volume was recorded every 24 h and then replaced with fresh SBF. To ensure the repeatability of experimental results, the experiment was repeated three times, and the average value of the measurements was recorded as a final result of each group. Additionally, the samples after soaking were characterized by SEM and XRD.

2.6. Cell Proliferation Assay and Cell Morphology Observation

To evaluate the cytocompatibility of the samples (AZ31, TA/AZ31, HA/AZ31, and HA/TA/AZ31), cell proliferation assays and cell morphology observations were used. The experiment was performed according to Lin [29] with a few changes. MC3T3-E1 cells were used to finish the experiment. Cells were cultured after one, four, and seven days in the leaching solution, respectively. Additionally, cells were cultured after one, four, and seven days in Dulbecco's modified Eagle's medium (DMEM) as negative group. Next, an MTT (3-(4, 5-dimethylthiazol-2-yl)-2, 5-diphenyltetrazolium bromide) test was completed to determine the cell proliferation. In order to quantitate the cell increment rate, the absorbance of each group was obtained using a microplate reader at 570 nm (Elx 800, Bio-Tek, Winooski, VT, USA), and the data were also subjected to an unpaired single tailed Student's *t*-test [30]. A value of $p < 0.05$ was considered as significant. The experiment was repeated three times to ensure the reliability of the results. Pictures of the cells at seven days were taken with an inverted optical microscope (IX2, Olympus, Tokyo, Japan).

3. Results and Discussion

3.1. SEM Analysis of the Samples

The SEM results of bare AZ31 magnesium alloys (AZ31), tannic acid-coated AZ31 (TA/AZ31), HA-coated AZ31 (HA/AZ31), and hydroxyapatite/tannic acid-coated AZ31 (HA/TA/AZ31) are shown in Figure 1a–d. The surface of the AZ31 is flat, and it has some apparent grinding scratches (Figure 1a). Compared to AZ31, the scratches of TA/AZ31 are also less pronounced (Figure 1b). This suggests that the tannic acid coating covers the scratches on the surface of the AZ31. Furthermore, the surface of the TA/AZ31 is a uniform structure with a small amount of cracking. The surface of HA/AZ31 (Figure 1c) clearly shows the chunks of calcium phosphate crystal and the surface is not uniform. However, the surface of the HA/TA/AZ31 is a brush-like array and porous (Figure 1d). Compared with the direct formation of HA, tannic acid can induce a more uniform HA coating, which may be attributed to the increase in the number of the centers of HA growth [19,20]. The pores in the HA/TA coating may be caused by hydrogen evolution [23,31]. The cross-section morphologies of the HA, TA, and HA/TA coatings are presented in Figure 1e–g, and the thickness of the coatings are shown in Table 1. The coatings of HA/AZ31 are thinner and looser than HA/TA/AZ31, which suggests that the tannic acid may promote the growth of HA on AZ31 magnesium alloys. In addition, the connection of HA/TA coating and substrate is closer than the direct formation of HA on AZ31 magnesium alloy surface. In the cross-section morphology of TA/AZ31 (Figure 1f), we can see there are two boundaries, one of them is between AZ31 Mg alloys and its tannic acid coating, the other one is between the tannic acid coating and the resin. Obviously, there exists a certain thickness between those two boundaries. This indicates that the surface of AZ31 forms a new coating according to the results of Chen et al. [24,26], namely a tannic acid coating.

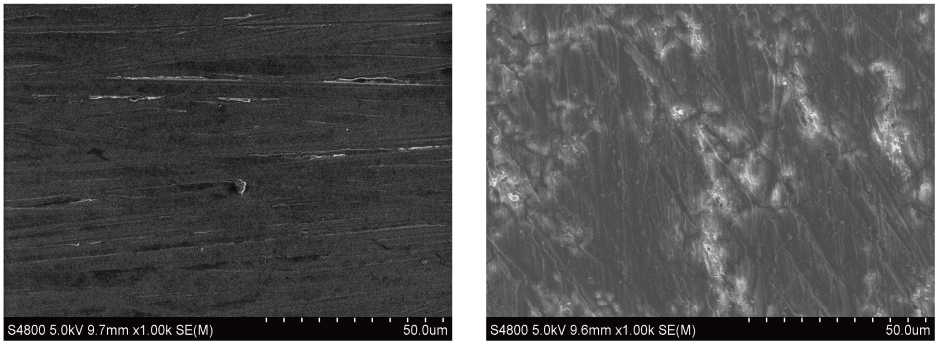

(**a**) (**b**)

Figure 1. *Cont.*

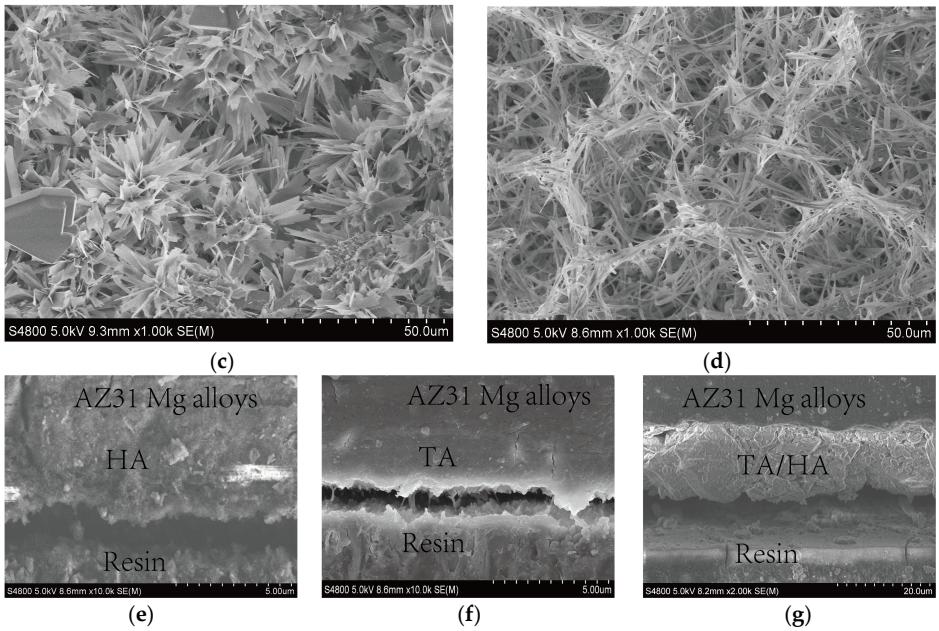

Figure 1. The SEM images showing the surface morphologies of (**a**) AZ31, (**b**) TA/AZ31, (**c**) HA/AZ31, (**d**) HA/TA/AZ31 and the cross-sections of (**e**) HA/AZ31, (**f**) TA/AZ31, and (**g**) HA/TA/AZ31.

Table 1. The coating thickness of HA/AZ31, TA/AZ31, and HA/TA/AZ31 (mean ± SD μm).

Samples	Thickness
HA/AZ31	4.66 ± 0.25
TA/AZ31	1.66 ± 0.22
HA/TA/AZ31	15.61 ± 0.64

The surface morphologies of AZ31, TA/AZ31, HA/AZ31, and HA/TA/AZ31 specimens after immersion in SBF for seven days are shown in Figure 2a–d. The surface of the bare AZ31 after soaking in SBF solution for seven days has a large number of wide, deep cracks and pits with a small amount of scattered spherical particles. Compared with bare AZ31 after soaking, the cracks and pits of the surface of tannic acid-coated AZ31 after soaking is significantly decreased, and the cracks and pits are narrower and shallower. The crack formation can be ascribed to water loss of the corrosion products and surface shrinkage [32]. In addition, the surface of tannic acid-coated AZ31 after soaking forms uniform, dense, spherical particles. The HA/AZ31 after soaking displays more obvious cracks compared to the HA/AZ31. However, compared to HA/AZ31 after soaking, the HA/TA/AZ31 after soaking became denser and the cracks and pits also apparently decrease. The results show that the samples after soaking underwent CaP redeposition.

The element compositions of the TA/AZ31, HA/TA/AZ31 surface are analyzed by EDS in Figure 3a,b. The C, O, and Mg are detected on two groups. The elements of C and O are detected on TA/AZ31 surface, which shows that there is a new coating on the surface of AZ31. Compared to TA/AZ31, Ca and P are detected on HA/TA/AZ31 surface, the atomic ratio Ca/P is 1.62, and this is close to that of hydroxyapatite (1.67). Additionally, the relatively low Ca/P also illustrates that Ca is insufficient in the HA/TA coating, and this may be due to a small amount of magnesium ions replacing the calcium ion in the HA [33]. According to Ren et al. [34], the replacement is good for mimicking natural bone tissue.

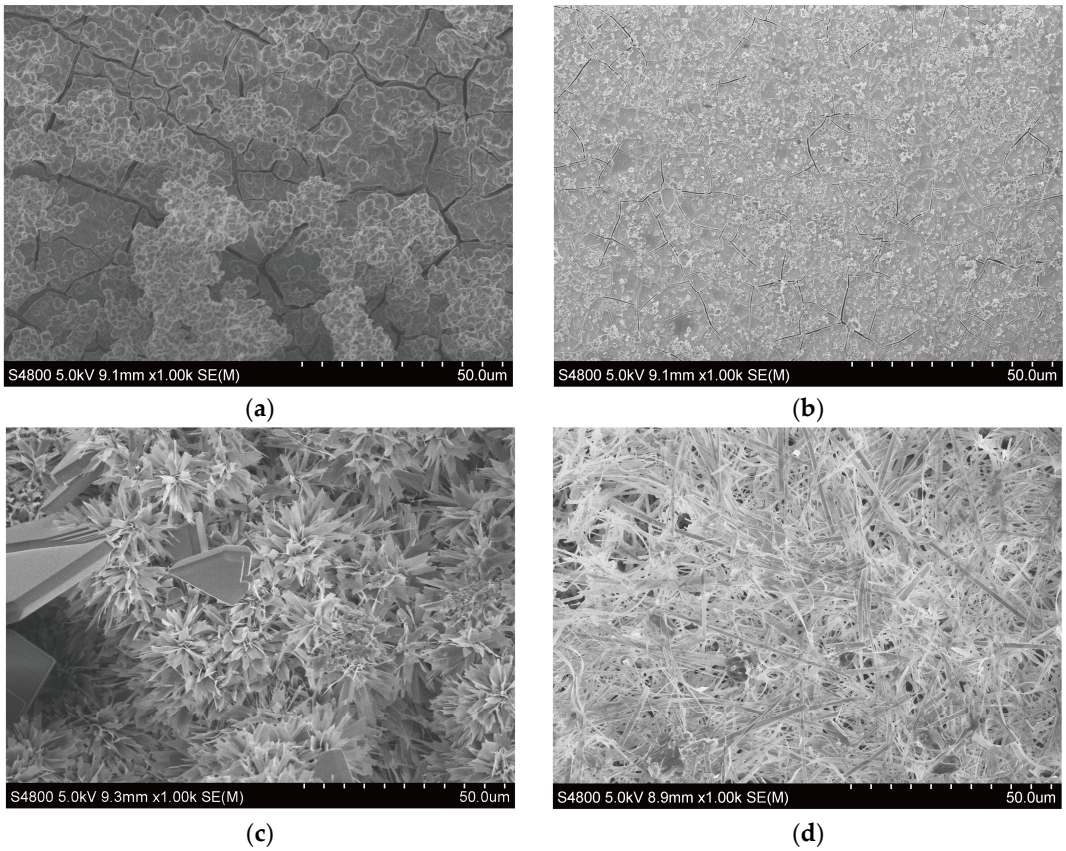

Figure 2. The SEM images showing the surface morphologies of AZ31 (**a**), TA/AZ31 (**b**), HA/AZ31 (**c**), and HA/TA/AZ31 (**d**) specimens after soaking 7 days in SBF.

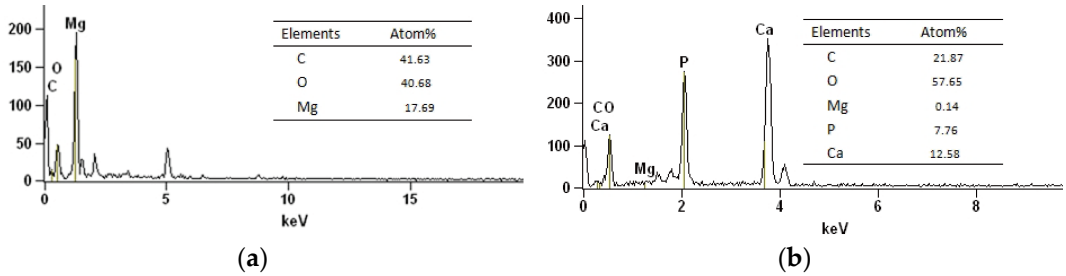

Figure 3. The elemental compositions of the TA/AZ31 (**a**) and HA/TA/AZ31 (**b**) surfaces are analyzed by EDS.

Figure 4 shows the XRD pattern of AZ31, TA/AZ31, HA/AZ31, and HA/TA/AZ31 specimens before (a, c, e, g) and after (b, d, f, h) soaking in SBF for seven days. The diffraction peaks of Mg are detected for all specimens. Furthermore, there is no obvious difference in the XRD patterns between AZ31 and TA/AZ31. This result may be caused by the non-crystallinity of the tannic acid coating [29]. In HA/TA/AZ31, new peaks are seen at $2\theta = 25.9°$, $29.1°$, $31.7°$, and $2\theta = 53.4°$ in the XRD pattern besides the AZ31 peaks, and these peaks originate from the (002), (210), (100), and (004) reflections of HA [29]. In addition, the some HA peaks are detected for all samples after being immersed for seven days, which is consistent with the scanning electron microscopy result (Figure 2a,b). Therefore, we infer that the surface of the AZ31 and TA/AZ31 after soaking forms a CaP coating in the SBF according to the study by Fragal et al. [35].

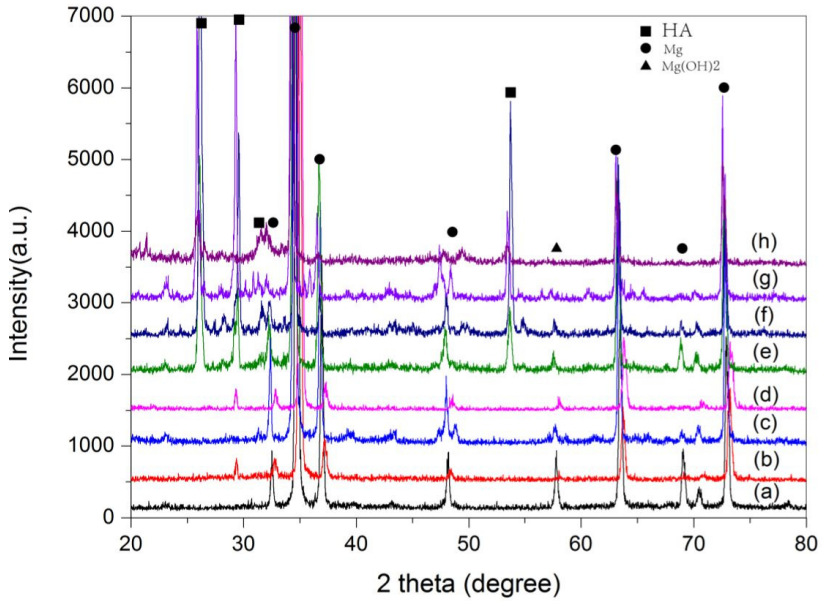

Figure 4. The XRD pattern of AZ31, TA/AZ31, HA/AZ31, and HA/TA/AZ31 specimens before (a, c, e, g) and after (b, d, f, h) soaking in SBF for 7 days.

The FTIR spectra of AZ31, TA/AZ31, HA/AZ31, and HA/TA/AZ31 are shown in Figure 5. For the TA/AZ31 sample, several characteristic peaks of benzene are seen at 1600–1450 cm^{-1}, and 1300–1000 cm^{-1} [26]. Therefore, the presence of the benzene ring peaks proves that the tannic acid film is successfully prepared on AZ31 Mg alloys by tannic acid treatment. For the HA/TA/AZ31 sample, the OH^- peak is seen at 3483 cm^{-1}, and the characteristic peaks of the phosphate group are detected at 1037 cm^{-1} and 561 cm^{-1} [29]. This indicates the formation of HA on tannic acid-coated AZ31 magnesium alloy surface. The carbonate band (CO_3^{2-}) at 1649 cm^{-1} and 870 cm^{-1} indicates that the hydroxyapatite structure contains carbonate ions. However, the special peaks of HA and TA coatings are not obvious in the spectrum of AZ31.

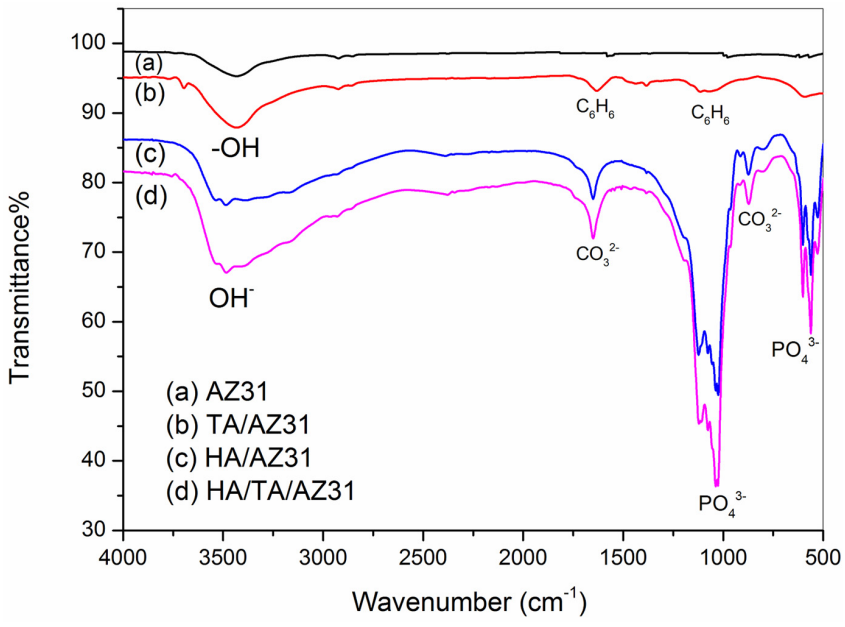

Figure 5. The FTIR spectra of (a) AZ31, (b) TA/AZ31, (c) HA/AZ31, and (d) HA/TA/AZ31.

The above material characterization results confirm the hydroxyapatite coating is formed on the AZ31 magnesium alloy with the assistance of tannic acid in the CaP solution. We infer that the formation is due to the hydroxyl groups of tannic acid adsorbing Ca^{2+} in solution, which forms positively-charged groups of the surface, and then many negatively-charged groups, such as OH^-, PO_4^{3-}, etc. in the solution combine with calcium ions. As a result, the AZ31 magnesium alloy surface forms the hydroxyapatite coating [35].

3.2. Corrosion Resistance Analysis

3.2.1. Polarization Measurements

The polarization curves, corrosion potential (E_{corr}), and corrosion current density (I_{corr}) of the AZ31, TA/AZ31, HA/AZ31, and HA/TA/AZ31 samples in SBF at 37 °C are shown in Figure 6 and Table 2, respectively. The HA-coated AZ31 has more positive E_{corr} (-1.391 ± 0.007 V) and lower I_{corr} ($(3.9337 \pm 0.2465) \times 10^{-7}$ A/cm^2) compared with the AZ31 substrate ($E_{corr} = -1.462 \pm 0.006$V, $I_{corr} = (4.8978 \pm 0.2455) \times 10^{-6}$ A/cm^2). However, the E_{corr} (-1.304 ± 0.006V) value of the HA/TA/AZ31 is the most positive, and its I_{corr} value ($(5.6494 \pm 0.3187) \times 10^{-8}$ A/cm^2) is the lowest. Compared with the bare AZ31, the E_{corr} for HA/TA/AZ31 was increased by about 158 mV, and the I_{corr} was decreased 100-fold. Therefore, the HA/TA coating can significantly improve the corrosion resistance of AZ31 compared to the TA coating and HA coating. This may be because the coating on the surface of the magnesium alloys blocks the corrosion ions from directly contacting the AZ31 magnesium alloy [36].

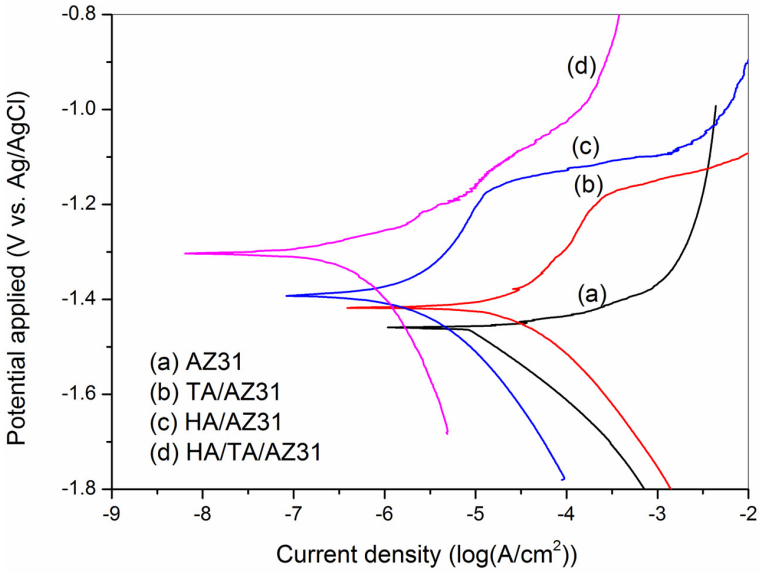

Figure 6. The PDP curves of (a) AZ31, (b) TA/AZ31, (c) HA/AZ31, and (d) HA/TA/AZ31 samples in SBF.

Table 2. The corrosion potential (E_{corr}) and corrosion current density (I_{corr}) of the AZ31, TA/AZ31, HA/AZ31, HA/TA/AZ31 samples in SBF at 37 °C (Mean ± SD).

Samples	E_{corr} (V)	I_{corr} (A/cm^2)
AZ31	-1.462 ± 0.006	$(4.8978 \pm 0.2455) \times 10^{-6}$
TA/AZ31	-1.416 ± 0.011	$(3.7334 \pm 0.3461) \times 10^{-6}$
HA/AZ31	-1.391 ± 0.007 *	$(3.9337 \pm 0.2465) \times 10^{-7}$ *
HA/TA/AZ31	-1.304 ± 0.006 *	$(5.6494 \pm 0.3187) \times 10^{-8}$ *

* The results of the group had significant difference related to AZ31 group ($p < 0.05$).

3.2.2. EIS Studies

Electrochemical impedance spectroscopy checks the charge transfer or hindrance at different phases. It can monitor the status and behavior of conducting phases interfaces [37]. Figure 7 shows the Nyquist plot for the bare, TA-coated, and HA/TA-coated AZ31 in SBF. Furthermore, the fitting equivalent circuits of the TA/AZ31 and HA/TA/AZ31 are shown in Figure 8a,b, respectively. Here, R_s represents the solution resistance of the system, R1 and C1, R2 and C2, and R3 and C3 represent the resistance and capacitance of bare AZ31, TA coating, and HA coating, respectively. This proves that HA/TA/AZ31 has two time constants that are attributed to the inner, dense TA coating and outer, porous HA. The polarization resistance (R_p) is 6203 Ω cm^2, 25,634 Ω cm^2, and 63,637 Ω cm^2 for AZ31, TA/AZ31, and HA/TA/AZ31, respectively. Compared with AZ31, the TA/AZ31 has a higher R_p value, which can be attributed to the effective protection of TA coating as the passivation film. However, the HA/TA double-coated AZ31 Mg alloys shows the largest value of the polarization resistance due to the superposition of the protection of double coating [31]. It is also clear that the Nyquist plot of the HA/TA/AZ31 has two capacitive semicircles—the first semicircle is attributed to the porous HA coating, and the second semicircle to the dense TA coating [31]. We infer that the HA/TA double coating can significantly improve the corrosion resistance of AZ31.

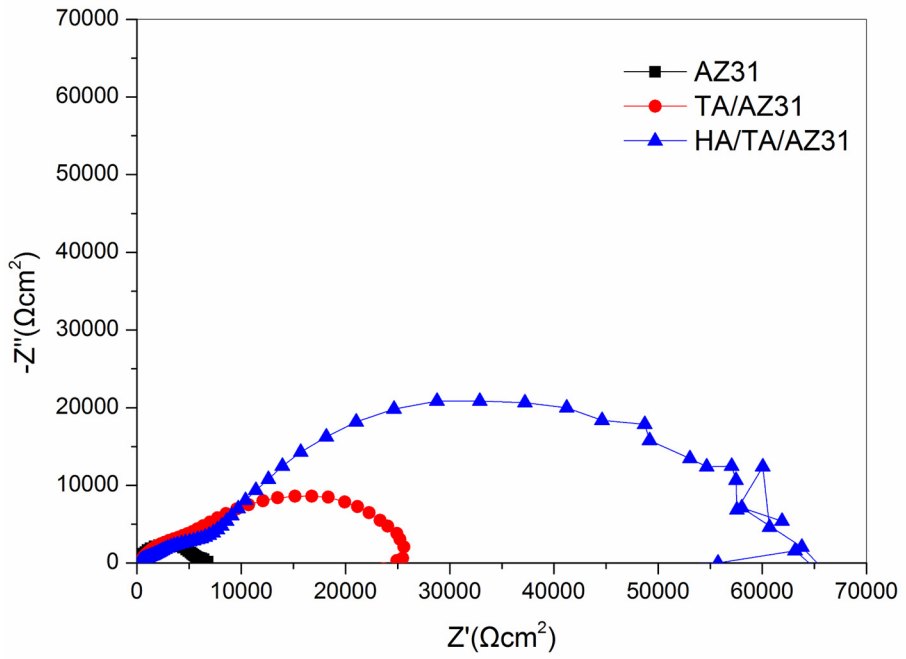

Figure 7. The Nyquist plot of the AZ31-, TA-, and HA/TA-coated samples in SBF.

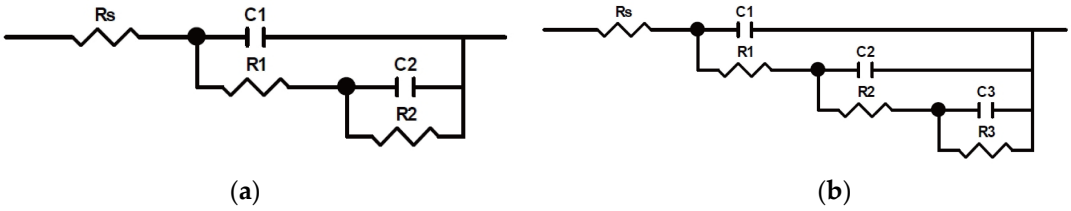

Figure 8. The fitting equivalent circuits of TA/AZ31 (**a**) and HA/TA/AZ31 (**b**).

3.2.3. H_2 Evolution Testing

Cumulative hydrogen gas evolution plots for the bare, TA-coated, HA-coated, and HA/TA-coated samples in the SBF solution for seven days at 37 °C are shown in Figure 9. The results show that

the bare AZ31 Mg alloys have the highest hydrogen evolution rate (0.52 mL/cm^2/day) during the immersion, while the hydrogen release rate of the HA-, TA-, and HA/TA-coated samples are 0.196, 0.363, and 0.161 mL/cm^2/day, respectively. This suggests that the corrosion of bare AZ31 Mg alloys in SBF solution is more likely to occur. However, TA and HA/TA films could significantly hinder the corrosion of AZ31 magnesium alloys, which is consistent with the potentiodynamic polarization data and EIS studies.

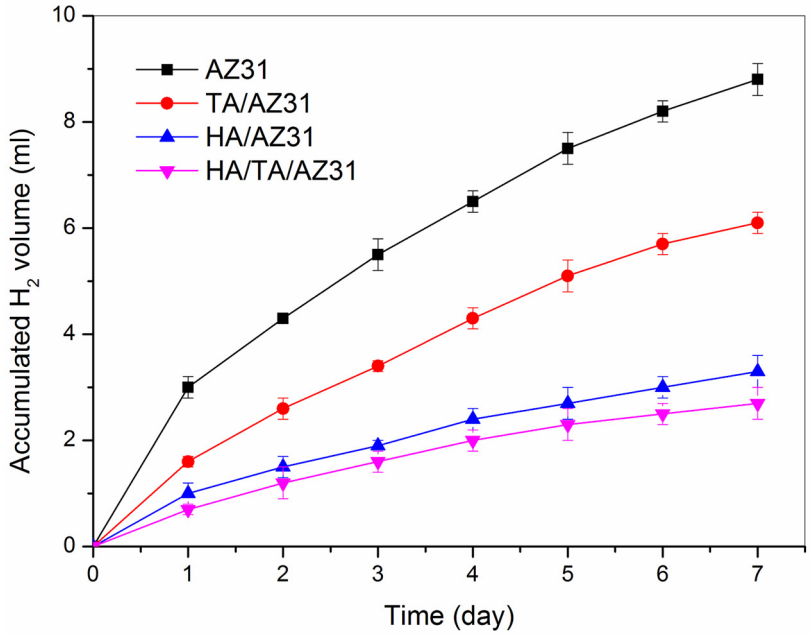

Figure 9. The hydrogen evolution volumes of AZ31, HA/AZ31, TA/AZ31, and HA/TA/AZ31 in SBF for seven days.

3.3. Cytotoxicity Evaluation

The MTT results assess the cytotoxicity of the AZ31, HA/AZ31, TA/AZ31, and HA/TA/AZ31 (Figure 10). The viabilities of MC3T3-E1 cells cultured with the extract media of AZ31, HA/AZ31, and HA/TA/AZ31 for 1, 4, and 7 d are higher than 80% suggest that the AZ31, HA/AZ31, and HA/TA/AZ31 samples are non-toxic. In particular, the cell viability of the HA/TA/AZ31 sample is higher than 100%. We infer that the HA coatings can improve the proliferation of MC3T3-E1 cells in vitro—this result is consistent with Lin et al. [29,38,39]. The reason that the dissolved HA from the coating might act as a growth factor to encourage proliferation of MC3T3-E1 cells [39,40] and the porous structure of HA/TA coating can accelerate the differentiation and proliferation of osteoblasts and promote new bone reconstruction [40]. However, the cell viability of TA/AZ31 after 1, 4, and 7 days is lower than 80%, indicating mild toxicity; this may be that tannic acid, as a fixed agent, can cause proteins and sugars in the cell membrane to be destroyed [41].

Figure 11 shows the morphologies of the MC3T3-E1 cells cultured in extraction medium from AZ31 (a), TA/AZ31 (b), HA/TA/AZ31 (c), and negative control (d) for seven days by optical microscopy. The amount of cells incubated in the extract medium of HA/TA/AZ31 and the negative group is significantly more than TA/AZ31 and AZ31, which suggests that HA improves the cytocompatibility of TA/AZ31 and AZ31. Compared to the negative control group, the morphologies of MC3T3-E1 cells cultured in the extract medium of TA/AZ31 are significantly different. This shows that the TA coating has slight cytotoxicity. The morphologies of MC3T3-E1 cells cultured in the extract of AZ31 and HA/TA/AZ31 are normal and healthy, which is similar to that of the negative control group. In terms of the results of cell morphology, the HA coating can significantly improve the cytocompatibility of AZ31 and TA/AZ31, which is consistent with the MTT results.

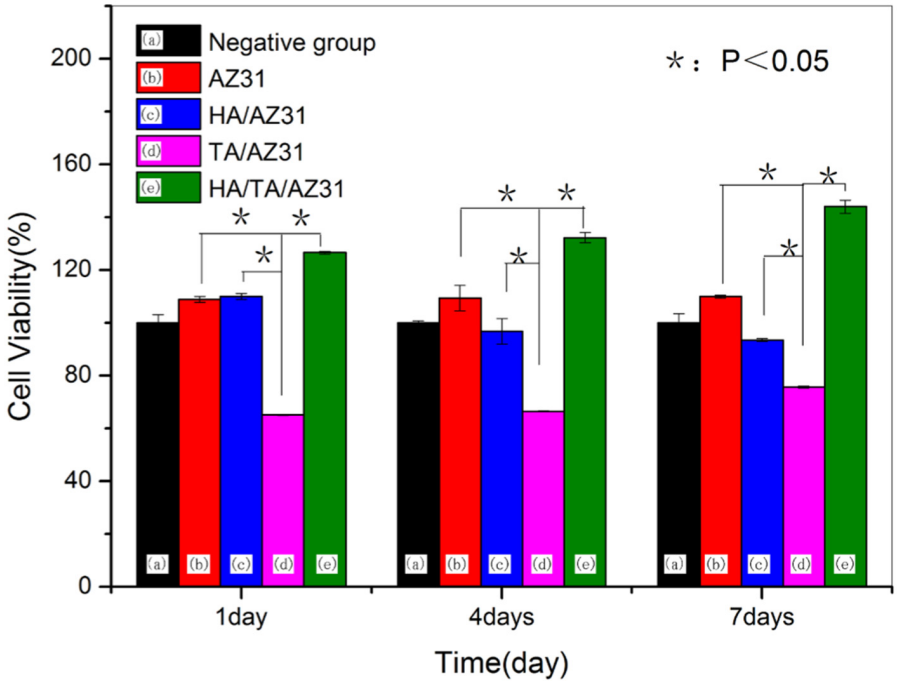

Figure 10. The cell viabilities of MC3T3-E1 cells cultured in extraction mediums of (a) negative group; (b) AZ31; (c) HA/AZ31; (d) TA/AZ31; and (e) HA/TA/AZ31.

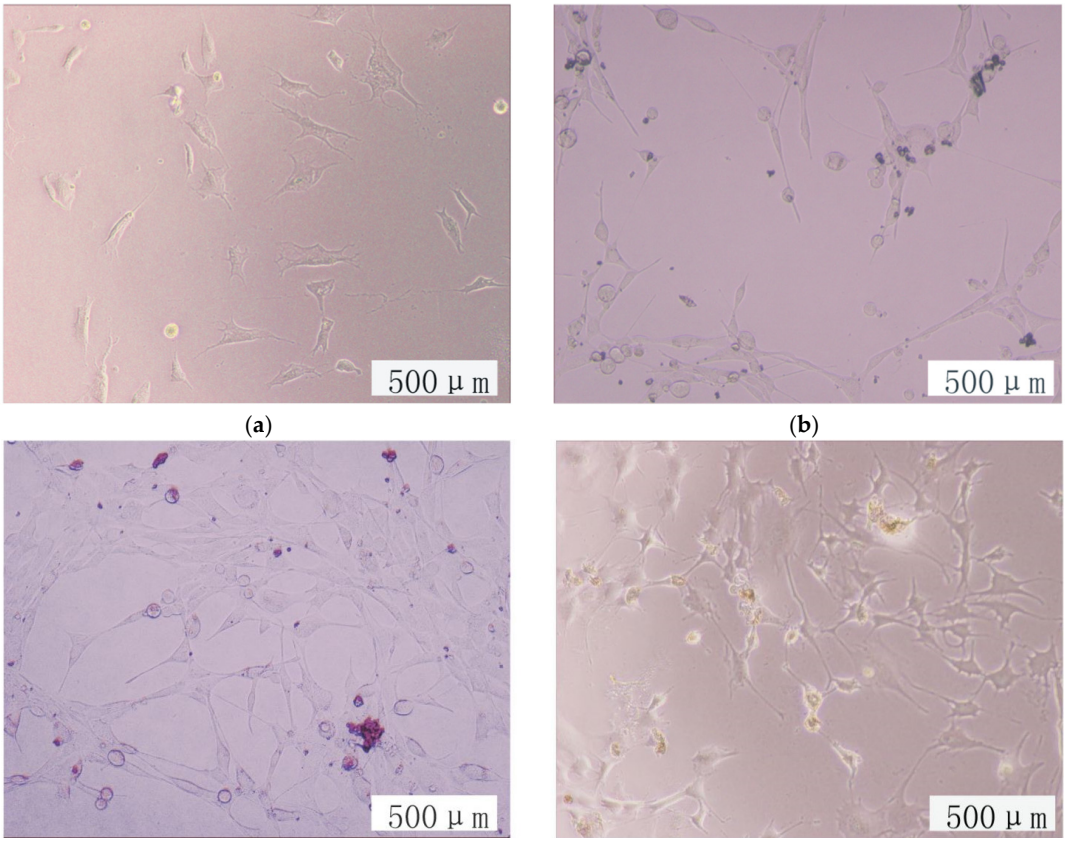

(**a**) (**b**)

(**c**) (**d**)

Figure 11. The optical microscopy images (20×) representing the morphologies of MC3T3-E1 cells cultured for 7 d in AZ31 (**a**), TA/AZ31 (**b**), and HA/TA/AZ31 (**c**) extracts, and the negative control (**d**).

4. Conclusions

The hydroxyapatite/tannic acid coatings on AZ31 magnesium alloys are successfully prepared by chemical conversion and biomimetic method. The corrosion resistance results reveal that the corrosion rate of the hydroxyapatite/tannic acid-coated AZ31 substrate is apparently decreased, which is beneficial to reduce the biodegradable rate of magnesium alloys. The cytotoxicity tests indicate that the HA/TA/AZ31 did not produce a cytotoxic response for MC3T3-E1 cells, and this promotes cell proliferation. The results verify that the formation of HA coatings on TA/AZ31 magnesium alloys to increase corrosion resistance and improve cytocompatibility is feasible.

Acknowledgments: This work was supported by the Natural Foundation of Gansu Province, China (grant no. 1208RJZA236), the Key Technology Support Program of Gansu Province, China (grant no. 1604FKCA089), and the Fundamental Research Funds for the Central Universities (grant no. lzujbky-2017-it48). We sincerely thank Zhenjun Peng from the State Key Laboratory of Solid Lubrication, Lanzhou Institute of Chemical Physics, Chinese Academy of Sciences for the technical assistance during these studies. We also appreciate the valuable comments provided by other members of our laboratories.

Author Contributions: Bowu Zhu, Jun Liang, and Baocheng Cao conceived and designed the experiments; Bowu Zhu performed the experiments; Bowu Zhu, Shimeng Wang, Lei Wang, and Yang Yang analyzed and discussed the data; Bowu Zhu wrote the paper; and Jun Liang and Baocheng Cao conducted the revision and direction of the work.

Conflicts of Interest: The authors declare no conflict of interest.

References

1. Hornberger, H.; Virtanen, S.; Boccaccini, A.R. Biomedical coatings on magnesium alloys—A review. *Acta Biomater.* **2012**, *8*, 2442–2455. [CrossRef] [PubMed]
2. Shadanbaz, S.; Dias, G.J. Calcium phosphate coatings on magnesium alloys for biomedical applications: A review. *Acta Biomater.* **2012**, *8*, 20–30. [CrossRef] [PubMed]
3. Yazdimamaghani, M.; Razavi, M.; Vashaee, D.; Tayebi, L. Development and degradation behavior of magnesium scaffolds coated with polycaprolactone for bone tissue engineering. *Mater. Lett.* **2014**, *132*, 106–110. [CrossRef]
4. Cui, W.; Beniash, E.; Gawalt, E.; Xu, Z.; Sfeir, C. Biomimetic coating of magnesium alloy for enhanced corrosion resistance and calcium phosphate deposition. *Acta Biomater.* **2013**, *9*, 8650–8659. [CrossRef] [PubMed]
5. Sydow-Plum, G.; Tabrizian, M. Review of stent coating strategies: Clinical insights. *Mater. Sci. Technol.* **2013**, *24*, 1127–1143. [CrossRef]
6. Raman, V.; Tamilselvi, S.; Rajendran, N. Electrochemical impedance spectroscopic characterization of titanium during alkali treatment and apatite growth in simulated body fluid. *Electrochim. Acta* **2007**, *52*, 7418–7424. [CrossRef]
7. Feng, J.; Chen, Y.; Liu, X.; Liu, T.; Zou, L.; Wang, Y.; Ren, Y.; Fan, Z.; Lv, Y.; Zhang, M. In-situ hydrothermal crystallization $Mg(OH)_2$ films on magnesium alloy AZ91 and their corrosion resistance properties. *Mater. Chem. Phys.* **2013**, *143*, 322–329. [CrossRef]
8. Wang, D.; Chen, C.; Ma, J.; Zhang, G. In situ synthesis of hydroxyapatite coating by laser cladding. *Colloids Surf. B* **2008**, *66*, 155–162. [CrossRef] [PubMed]
9. Song, Y.; Zhang, S.; Li, J.; Zhao, C.; Zhang, X. Electrodeposition of Ca-P coatings on biodegradable Mg alloy: In vitro biomineralization behavior. *Acta Biomater.* **2010**, *6*, 1736–1742. [CrossRef] [PubMed]
10. Song, Y.; Shan, D.; Han, E. Electrodeposition of hydroxyapatite coating on AZ91D magnesium alloy for biomaterial application. *Mater. Lett.* **2008**, *62*, 3276–3279. [CrossRef]
11. Gyorgy, E.; Grigorescu, S.; Socol, G.; Mihailescu, I.N.; Janackovic, D.; Dindune, A.; Kanepe, Z.; Palcevskis, E.; Zdrentu, E.L.; Petrescu, S.M. Bioactive glass and hydroxyapatite thin films obtained by pulsed laser deposition. *Appl. Surf. Sci.* **2007**, *253*, 7981–7986. [CrossRef]
12. Oliveira, A.L.; Reis, R.L.; Li, P. Strontium-Substituted Apatite Coating Grown on Ti_6Al_4V Substrate Through Biomimetic Synthesis. *J. Biomed. Mater. Res. Part B* **2007**, *330–332*, 258–265. [CrossRef] [PubMed]

13. Kawashita, M.; Itoh, S.; Miyamoto, K.; Takaoka, G.H. Apatite formation on titanium substrates by electrochemical deposition in metastable calcium phosphate solution. *J. Mater. Sci. Mater. Med.* **2008**, *19*, 137–142. [CrossRef] [PubMed]
14. Chung, C.J.; Long, H.Y. Systematic strontium substitution in hydroxyapatite coatings on titanium via micro-arc treatment and their osteoblast/osteoclast responses. *Acta Biomater.* **2011**, *7*, 4081–4087. [CrossRef] [PubMed]
15. Manso, M.; Jiménez, C.; Morant, C.; Herrero, P.; Martínez-Duart, J.M. Electrodeposition of hydroxyapatite coatings in basic conditions. *Biomaterials* **2000**, *21*, 1755–1761. [CrossRef]
16. Zhao, C.; Fan, H.; Zhang, X. Advances in Biomimetic Apatite Coating on Metal Implants. In *Advances in Biomimetics*; George, A., Ed.; InTech: Rijeka, Croatia, 2011.
17. Gao, F.; Xu, C.; Hu, H.; Wang, Q.; Gao, Y.; Chen, H.; Guo, Q.; Chen, D.; Eder, D. Biomimetic synthesis and characterization of hydroxyapatite/graphene oxide hybrid coating on Mg alloy with enhanced corrosion resistance. *Mater. Lett.* **2015**, *138*, 25–28. [CrossRef]
18. Fang, B.; Wan, Y.; Tang, T.; Gao, C.; Dai, K. Proliferation and Osteoblastic Differentiation of Human Bone Marrow Stromal Cells on Hydroxyapatite/Bacterial Cellulose Nanocomposite Scaffolds. *Tissue Eng. Part A* **2009**, *15*, 1091–1098. [CrossRef] [PubMed]
19. Cellet, T.P.; Pereira, G.M.; Muniz, E.C.; Silva, R.; Rubira, A.F. Hydroxyapatite Nanowhiskers Embedded in Chondroitin Sulfate Microspheres as Colon Targeted Drug Delivery System. *J. Mater. Chem. B* **2015**, *3*, 6837–6846. [CrossRef]
20. Silva, R.; Pereira, G.M.; Muniz, E.C.; Rubira, A.F. Calcium Carbonate Crystallization on a Polyethylene Surface Containing Ultrathin Layers of Hydrophilic Polymers. *Cryst. Growth Des.* **2009**, *9*, 3307–3312. [CrossRef]
21. Dollman, D.Y. Method and Compositions for Coating Aluminum. U.S. Patent 4,191,596, 1980.
22. Gust, J.; Suwalski, J. Use of Mössbauer Spectroscopy to Study Reaction Products of Polyphenols and Iron Compounds. *Corrosion* **1994**, *50*, 355–365. [CrossRef]
23. Zuo, X.; Li, W.; Mu, S.; Du, J.; Yang, Y.; Tang, P. Investigation of composition and structure for a novel Ti–Zr chemical conversion coating on 6063 aluminum alloy. *Prog. Org. Coat.* **2015**, *87*, 61–68. [CrossRef]
24. Chen, X.; Li, G.; Lian, J.; Jiang, Q. An organic chromium-free conversion coating on AZ91D magnesium alloy. *Appl. Surf. Sci.* **2008**, *255*, 2322–2328. [CrossRef]
25. Keim, S.; Brunner, J.G.; Fabry, B.; Virtanen, S. Control of magnesium corrosion and biocompatibility with biomimetic coatings. *J. Biomed. Mater. Res. Part B* **2011**, *96*, 84–90. [CrossRef] [PubMed]
26. Chen, X.; Li, G.; Lian, J.; Jiang, Q. Study of the formation and growth of tannic acid based conversion coating on AZ91D magnesium alloy. *Surf. Coat. Technol.* **2009**, *204*, 736–747. [CrossRef]
27. Kokubo, T.; Takadama, H. How useful is SBF in predicting in vivo bone bioactivity? *Biomaterials* **2006**, *27*, 2907–2915. [CrossRef] [PubMed]
28. Bakhsheshi-Rad, H.R.; Hamzah, E.; Kasiri-Asgarani, M.; Jabbarzare, S.; Iqbal, N.; Abdul-Kadir, M.R. Deposition of nanostructured fluorine-doped hydroxyapatite-polycaprolactone duplex coating to enhance the mechanical properties and corrosion resistance of Mg alloy for biomedical applications. *Mater. Sci. Eng. C Mater. Biol. Appl.* **2016**, *60*, 526–537. [CrossRef] [PubMed]
29. Lin, B.; Zhong, M.; Zheng, C.; Cao, L.; Wang, D.; Wang, L.; Liang, J.; Cao, B. Preparation and characterization of dopamine-induced biomimetic hydroxyapatite coatings on the AZ31 magnesium alloy. *Surf. Coat. Technol.* **2015**, *281*, 82–88. [CrossRef]
30. Li, X.; Li, S.; Zhang, M.; Zhang, W.; Li, C. Evaluations of Antibacterial Activity and Cytotoxicity on Ag Nanoparticles. *Rare Metal Mater. Eng.* **2011**, *40*, 209–214.
31. Gopi, D.; Ramya, S.; Rajeswari, D.; Kavitha, L. Corrosion protection performance of porous strontium hydroxyapatite coating on polypyrrole coated 316L stainless steel. *Colloids Surf. B* **2013**, *107*, 130–136. [CrossRef] [PubMed]
32. Bakhsheshi-Rad, H.R.; Hamzah, E.; Daroonparvar, M.; Saud, S.N.; Abdul-Kadir, M.R. Bi-layer nano-TiO_2/FHA composite coatings on Mg–Zn–Ce alloy prepared by combined physical vapour deposition and electrochemical deposition methods. *Vacuum* **2014**, *110*, 127–135. [CrossRef]
33. Habibovic, P.; Barrère, F.; Blitterswijk, C.A.V.; Groot, K.D.; Layrolle, P. Biomimetic Hydroxyapatite Coating on Metal Implants. *J. Am. Ceram. Soc.* **2002**, *85*, 517–522. [CrossRef]

34. Ren, Y.; Zhou, H.; Nabiyouni, M.; Bhaduri, S.B. Rapid coating of AZ31 magnesium alloy with calcium deficient hydroxyapatite using microwave energy. *Mater. Sci. Eng. C Mater. Biol. Appl.* **2015**, *49*, 364–372. [CrossRef] [PubMed]
35. Fragal, E.H.; Cellet, T.S.; Fragal, V.H.; Companhoni, M.V.; Ueda-Nakamura, T.; Muniz, E.C.; Silva, R.; Rubira, A.F. Hybrid materials for bone tissue engineering from biomimetic growth of hydroxyapatite on cellulose nanowhiskers. *Carbohydr. Polym.* **2016**, *152*, 734–746. [CrossRef] [PubMed]
36. Arukalam, I.O.; Madufor, I.C.; Ogbobe, O.; Oguzie, E.E. Adsorption and inhibitive properties of hydroxypropyl methylcellulose on the acid corrosion of mild steel. *Int. J. Appl. Sci. Eng. Res.* **2013**, *2*, 613–629.
37. Conway, B.E. *Electrochemical Supercapacitors Scientific Fundamentals and Technological Applications*; Kluwer Academic/Plenum Publishers: New York, NY, USA, 1999; p. 210.
38. Cao, L.; Wang, L.; Fan, L.; Xiao, W.; Lin, B.; Xu, Y.; Liang, J.; Cao, B. RGDC Peptide-Induced Biomimetic Calcium Phosphate Coating Formed on AZ31 Magnesium Alloy. *Materials* **2017**, *10*, 358. [CrossRef]
39. Abdal-Hay, A.; Amna, T.; Lim, J.K. Biocorrosion and osteoconductivity of PCL/nHAp composite porous film-based coating of magnesium alloy. *Solid State Sci.* **2013**, *18*, 131–140. [CrossRef]
40. Laurencin, D.; Almora-Barrios, N.; de Leeuw, N.H.; Gervais, C.; Bonhomme, C.; Mauri, F.; Chrzanowski, W.; Knowles, J.C.; Newport, R.J.; Wong, A. Magnesium incorporation into hydroxyapatite. *Biomaterials* **2011**, *32*, 1826–1837. [CrossRef] [PubMed]
41. Liu, X.; Kim, J.K.; Li, Y.; Li, J.; Liu, F.; Chen, X. Tannic acid stimulates glucose transport and inhibits adipocyte differentiation in 3T3-L1 cells. *J. Nutr.* **2005**, *135*, 165–171. [PubMed]